The Deformation of a SLM Porous Titanium printed Acetabular Implant

A Conceptual Design

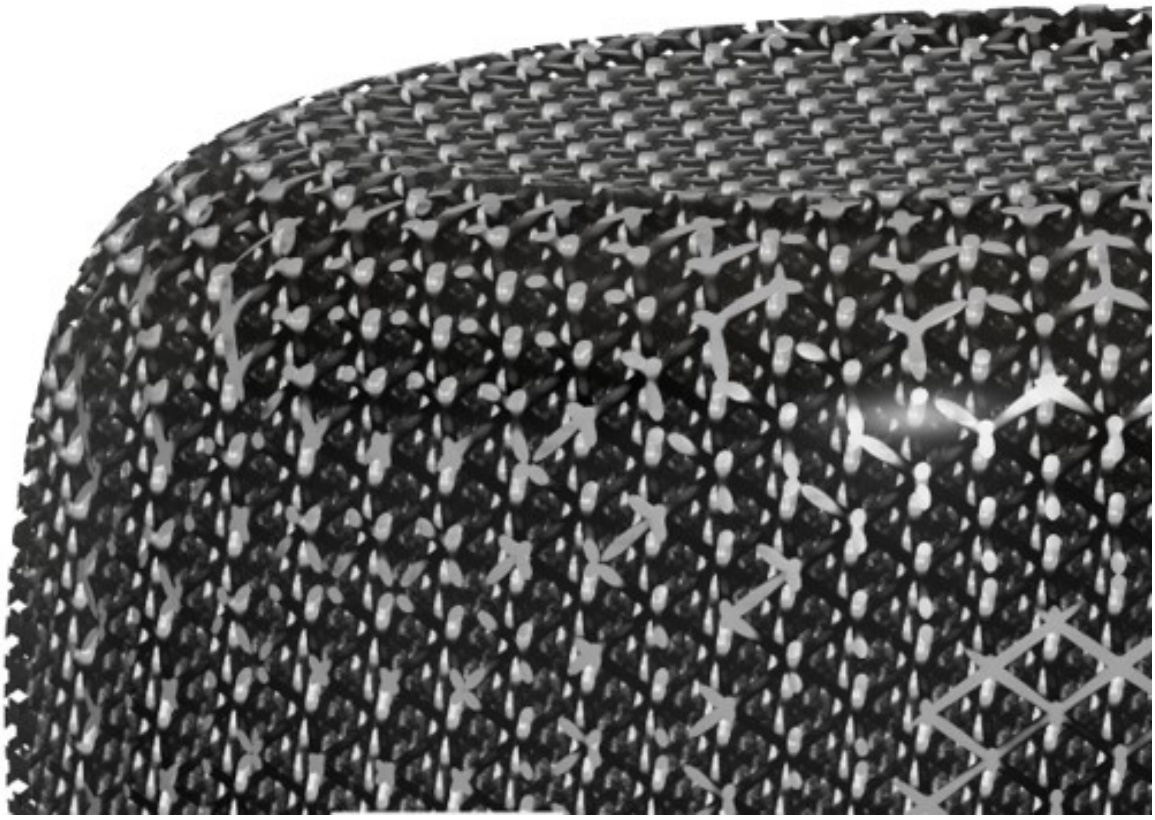

Thijmen van der Hulst August 20, 2024

Table of Contents

List of Tables

Nomenclature

Abbreviations

AM	Additive Manufacturing
CAD	Computer-Aided-Design
FDM	Fused Deposition Modelling
SLA	Stereolithography
SLS	Selective Laser Sintering
SLM	Selective Laser Melting
ABS	Acrylonitrile Butadiene Styrene
PLA	Polyactic Acid
BCC	Body-Centered Cubic
CP-Ti	Commercially Pure Titanium
ISO	International Organization for Standardization
THA	Total Hip Arthroplasty
ANOVA	Analysis Of Variance
LS	Lateral Strain
AS	Axial Strain
HIP	Hot Isostatic Pressing

Symbols

L	Strut Length (mm)
U	Unit Cell Size (mm)
θ	Angle in Degrees Between Struts
E	Young's Modulus (Pa)
ε	Strain
σ	Stress (Pa)
H	Height of the Weight Load Cell (meter)
E_k	Kinetic Energy (Joule)
G	Gravitational Constant (9.81 m/s^2)
M	Weight Load Cell (kg)

Equations

Equation 1: Diamond - Strut Length

$$L = \frac{3U}{4\sqrt{3}} = \frac{U}{2\sqrt{2}\cos(\theta)}, \text{ given } \theta = 35.26^\circ$$

Equation 2: BCC - Strut Length

$$L = \frac{\sqrt{3U^2}}{2}$$

Equation 3: Elastic Modulus

$$E = \frac{\sigma}{\varepsilon}$$

Equation 4: Height of Impact Load Cell

$$H = \frac{E_k}{GM}$$

Preface

At first I want to thank my supervisors Edsko Hekman, Nico Verdonschot and Chien NGuyen for their guidance in this study. Due to their mentorship, help and feedback I was able to structure my process, interpret processes and gain knowledge concerning the different aspects present in this master thesis.

Furthermore, I want to give my gratitude to the members of the 3D Lab at UMC Utrecht: Joëll Magré, Koen Willemsen and Harrie Weinans. Their feedback helped me in understanding the design case and in reflecting on my results and interpretations.

Also, I want to thank Christopher Balfe for making the use of the ARAMIS system and the Zwick/Roell compression machine and possible, and taking all the time to support in doing so. Also, I want to thank Bert Vos for enabling the execution of the drop test.

I like to acknowledge and thank the company AMNOVIS for manufacturing the samples tested in this research.

My appreciation goes to the trainees and graduating students of the 3D Lab which helped me in solving practical issues and made my time at the UMC Utrecht most enjoyable.

Abstract

This study involved the suggestion of a SLM printed CP-Ti grade 1 mesh to be implemented in a Paprosky 3A defect during a revision THA surgery. In pursuing this design goal, BCC- and diamond lattices were included in mesh designs and analysed in their material response to uniaxial impact and uniaxial static compression. The potential of osseointegration was described also. The different designs varied in the appliance of lattice structure and length/thickness strut ratio. During all executions of experiments no disengaged struts were identified. Moreover, BCC based meshes showed promise in offering surgeons more flexibility during impactation of material. Furthermore, diamond designs with a ratio of 5 displayed significant lateral expansion through uniaxial static compression. However, other diamond based designs failed in establishing considerable lateral expansion due to low yield stresses establishing a fast collapse of material. BCC designed meshes containing a ratio of 10 and 15 provided considerate lateral expansion as well. Considering the potential of osseointegration, BCC derived meshes with a ratio of 15 and diamond derived meshes with a ratio of 10 and 15 provided elastic moduli and yield stresses comparable to surrounding bone tissue present in a Paprosky 3A defect. Resulting pore sizes after imapct and static compression were in accordance with the set requirements. However, diamond based designs showed most promise due to the resulting pore morphology and stochastic structure.

1 Introduction

1.1 Research Background

Periprosthetic acetabular bone loss poses a significant challenge in revision THA(Total Hip Arthroplasty) procedures due to the applied fixations. The fixations used redistribute the load of the acetabular cup. The resulting change of stress signals the body to adapt the present bone quality accordingly. Consequently, a decline in bone density occurs, making the surrounding bone tissue more susceptible to fracture. This process is referred to as the stress-shielding phenomenon. As deficiencies occur due to the stress-shielding effect, revison THA surgery may be required over time. However, revision THA surgeries pose an elevated risk of failure. Especially the risk of failure amongst elderly is high due to their already low bone density [1].

While certain countries such as the United Kingdom and France may witness population growth attributed to increasing immigration and fertility rates, the global aging of populations [2], for instance in Italy and Russia, establish a prevailing trend in the number of elderly, consequently resulting in an increase of THA procedures in forthcoming decades. Germany and the United States of America are already enduring the complications of an aging population and the additional necessity of primary- and revision THA surgeries [3]. Research shows a projected increase of 62% in primary THA procedures and a 40% increase in revision THA procedures in Germany by 2060. The United States of America is anticipated to observe a 137% increase in revision THA procedures between 2005 and 2030 [3, 4].

A primary THA procedures involve the reaming of the acetabular socket to align and insert a jumbo cup appropriate to the patient's anatomy. The required intricate fixation is enforced through line-to-line fixation, screws, and bone cement. A shortcoming of these standardized procedures is the type of fixation. The cup tends to distribute the load it carries in a transverse direction, channelling the load toward the side and edge of the acetabular socket [5]. Wolff's law argues that bone tissue adapts by altering its density, structure, and shape in response to the imposed loads and stresses, thus elucidating the heightened probability of substantial bone resorption resulting in the stress-shielding phenomenon, and causing a probable increase in pain and inflammation.

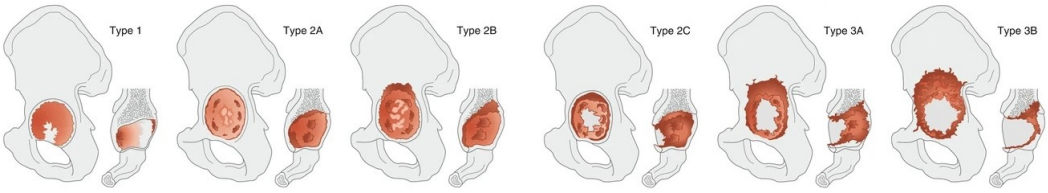

Figure 1: Paprosky classification of acetabular bone defects (lateral- and crosssectional view)[6]

The Paprosky classification system was created to accurately assess the morphology- and extent of this bone resorption, see figure 1. The system found its origin through clinical observations regarding extensive bone resorption and disturbances in the supporting bone structures of the acetabulum. Over time, the Paprosky methodology has gained widespread acknowledgment for effectively categorizing various levels of these bone defects [7, 8, 9]. Furthermore, the classification system has proven instrumental in identifying solutions based on the type of bone defect by informing a surgeon whether a standard fixation method of the cup remains optional or should be discarded.

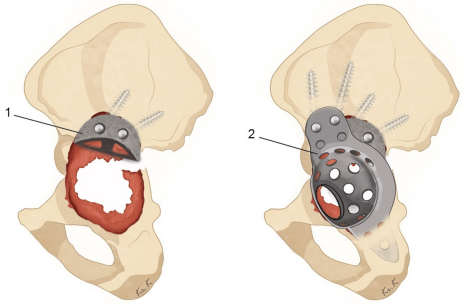

Figure 2: Use of a metal augment in a Paprosky 3B defect : (1) metal augment fixation, (2) cage fixation [10]

When a standard shell can not provide the required stability of a jumbo cup (Paprosky 3A/Paprosky 3B), the surgeon has a variety of tools available. These include the use of bone allografts, cages and various metal augments [11, 12, 13, 14]. Bone allograft is tissue harvested from a donor, used to fill extensive defects and facilitate regeneration of bone tissue. Metal augments serve to cover gaps surrounding the acetabular cup, see figure 2, and come in various shapes and sizes. Furthermore, metallic cages are employed in hip surgery to bridge substantial bone defects, and like the metal augment constructs, are engineered to be securely fixed onto the remaining healthy bone tissue, see figure 2. The use of these options is not ideal. They are not customized to the individual's anatomy and won't tackle the main cause of bone resorption, an even load distribution on the surface of the acetabular socket.

To address this challenge, greater attention has been directed at a more patient-specific acetabular cup design. These implants [16, 17] involve designing a cup accustomed to the patient's unique anatomy. Nevertheless, achieving an ideal fit remains challenging as minor discrepancies can lead to poor fitment. To prevent this issue, these designs incorporate an undersized cup with flanges. The flanges attach the implant to the Ischium, Ilium, and Pubis, providing additional stability. An example of such a customized (triflanged) cup is shown in figure 3. Still, using an undersized cup results in fixations penetrating healthy bone tissue and a limited contact surface between the surrounding bone tissue and the cup.

Figure 3: Custom made triflanged cup [15]

To tackle the lack of surface interaction between the cup and the fractured acetabular socket, the design of a highly porous deformable mesh shows promise. This approach suggests that an orthopedic surgeon could press a deformable mesh into an acetabular bone defect. By doing so, the need for allografts, cages, and metal augments will be eliminated in revision THA surgeries and thereby sparing additional damage to healthy bone tissue while expanding the surface contact area between the cup implant and surrounding bone tissue. Especially lattice-based meshes provide potential for such deformable meshes. As lattice structures are metamaterials, uncommon properties like a negative Poisson ratio or the combination of a low stiffness- but high strength complex could be realized. These unique properties can be applied on a deformable mesh by adjusting the lattice unit cell accordingly [18]. Metamaterials are categorized into auxetic- and non-auxetic metamaterials. Auxetic metamaterials, contain a negative Poisson ratio and therefore contract when being compressed. However, non-auxetic metamaterials, characterized by a positive Poisson's ratio, are most interesting in the case of designing bone substituting meshes. This is due to the capability of providing a high strength structure while also successfully

mimicking the less dense surrounding bone tissue. In engineering a micro-scale design, elements such as porosity can also be adjusted to facilitate the ingrowth of surrounding tissue [19]. Due to a wide variety in micro-scale design opportunities researchers often classify lattice structures in one-, or even multiple different categories. These classifications involve the mechanical properties, the morphology of the lattice construct, or the geometrical distribution [20]. Considering the mechanical properties, Gibson and Ashby (1982) developed a model that correlates the yield strength and elastic modulus for basic unit cells [21]. The morphology type determines whether a lattice structure is surface-based or strut-based. Surface-based lattices provide a large surface area that enhances cell adhesion and supports osseointegration. However, fabricating these lattices through additive manufacturing (AM) is more challenging, which affects the consistency and quality of the implant. In contrast, strut-based lattices facilitate direct load transfer, stimulating bone growth, and are easier to fabricate through AM due to their simpler structure, ensuring a consistent quality of the deformable mesh. Finally, the geometry of the mesh should also be considered in the micro-scale design. In this context, the choice between using a stochastic or a non-stochastic structure needs to be made. A stochastic lattice, with its irregular unit cells, can offer high compressive strength. However, its irregularity makes it more challenging to control the design features of the mesh. Conversely, a non-stochastic structure allows for more precise adjustments of material properties and provides greater flexibility in modifying shape features, including pore size [20].

Manufacturing deformable lattice-based meshes is most preferably executed through AM. This is due to the possibility of fabricating high quality complex geometries. A standard AM involves the use of a computer-aided-design (CAD) software to model a deformable mesh. Once a design is complete, additional software is applied to segment the model into slices. At last an AM-machine will print these slices in order. Given the printing process, many techniques have become available over time. In the design of biomedical applications Fused Deposition Modeling (FDM), Stereolithography (SLA), Selective Laser Sintering (SLS), Selective Laser Melting (SLM), and 3D Inkjet Printing have been applied frequently. FDM makes use of filaments made of Acrylonitrile Butadiene Styrene (ABS), Polylactic Acid (PLA), and Nylon. The method is fast but produces samples with weak mechanical properties. SLA polymerizes epoxy resins, manufacturing models with high accuracy and a fine surface finish. However, SLA has a high uncertainty when considering the mechanical properties of a sample. Furthermore, SLA is considered to be a highly expensive manufacturing process. SLS and SLM are high-resolution methods which apply lasers or high-energy beams to solidify metal powders. Both printing techniques have proven succesfull in the manufacturing of medical applications. As both techniques may be quite similar, a main difference can be found in the approach to the solidification process of the metal resins. While SLS uses sintering to heat the surface of the metallic powders to fuse together, SLM makes use of melting, thus raising the temperature of the powder above its melting temperature and fully fuse the metal powders. In doing so SLM is most promising in producing highly porous titanium models/meshes [22, 23, 24].

The design of a deformable lattice-based metallic mesh used to fill acetabular defects remains challenging, yet the use of a BCC- and diamond lattice frameworks, see figure 4, have already been applied and shown potential due to their high strength-to-weight ratio and corresponding stiffness [25]. Still, literature has been limited in comparing the different lattice frameworks. Given a Paprosky 3A scenario, a lattice titanium mesh will be required to occupy the areas of bone loss and stimulate osseointegration through transferring the load to the surrounding surface with a fitting pore structure. This research will concentrate on finding an optimal deformable titanium lattice mesh given a Paprosky 3A scenario.

Figure 4: BCC- and Diamond Unit Cell Structure [26]

1.2 Research Questions and Design Requirements

1.2.1 Research Question

To establish a confined design space, the subject of this research was defined. Within this process, the identification of the lattice structure type, the context of the design, and the intended objectives were essential. Consequently, this resulted in the formulation of the following research question:

Which deformable porous Titanium SLM printed acetabular mesh, under static- and impact compression, in a Paprosky 3A situation, will be most suitable to ensure the implant will shape itself to the acetabular socket anatomy of the patient during a hip (re-)revision operation and remain anchored, without the complete breakage of struts?

To answer this research question, the question at hand was deconstructed into three sub-questions. The sub-questions themselves were deconstructed to maintain a structural approach and address the contributing factors:

1. *How will the material respond given the provided impact by the surgeon in a hip revision surgery given a Paprosky 3A situation?*
    - 1.1. *Will there be a complete breakage of struts during impaction enforced by the surgeon during hip revision surgery in a Paprosky 3A situation?*
    - 1.2. *How will the material deform during impaction enforced by the surgeon during hip revision surgery in a Paprosky 3A situation?*
        - 1.2.1. *How will the material give in to the impact strikes provided by the surgeon during hip revision surgery in a Paprosky 3A situation?*
        - 1.2.2. *How will the material structure adapt itself to the impact strikes provided by the surgeon in a hip revision surgery given a Paprosky 3A situation?*
2. *How will the material respond given static compression forces provided by the surgeon and skeletal system in a Paprosky 3A situation?*
    - 2.1. *Will there be complete breakage of struts during static compression enforced by the surgeon during hip revision surgery in a Paprosky 3A situation?*
    - 2.2. *How will the designed material deform during static compression enforced by the surgeon during a hip revision surgery in a Paprosky 3A situation?*
        - 2.2.1. *How does the material enforce itself to the surface during static compression enforced by the surgeon in a hip revision surgery given a Paprosky 3A situation?*
        - 2.2.2. *How will the material plastically deform during static compression enforced by the surgeon during hip revision surgery in a Paprosky 3A situation?*
3. *How will the impacted material ensure potential osseointegration, given a Paprosky 3A situation?*
    - 3.1. *How will the material imitate the surrounding bone tissue?*
    - 3.2. *How will the material stimulate bone ingrowth?*

1.2.2 Set of Requirements

To answer the previously defined research questions, the design process requires a set of requirements to evaluate it's potential. This was accomplished through the use of the Functional Requirement model [27], a method used to describe the specific product functionalities. This model includes 4 domains, and the necessity of the different demands.

The first domain involves the mechanical properties. The mechanical properties of the mesh must match those of the surrounding bone tissue. A key component involves the elastic modulus, which is a measure of stiffness within the elastic region of deformation. A mesh with a high elastic modulus bears most of the load, thus failing in transferring the load to surrounding bone tissue. As this could result in bone resorption, the elastic modulus must approach the modulus of surrounding bone tissue. However, bone tissue contains a high level of anisotropy, and additonally the defect will be located in the acetabular socket, consisting of three different bone segments (Ischium, Ilium, and Pubis). For this reason a high variation of advised elastic moduli is defined in literature, consequently resulting in a wide range of 0.83 MPa to 89 MPa probable elastic moduli[28, 29, 30, 31]. Therefore a wide set of elastic moduli is to be considered (see Table 1). Given the situation of a Paprosky 3A situation, most bone loss will occur in the Ilium in a cranial direction. Therefore, the set of most identical elastic moduli can be refined. The Young's modulus of the Ilium ranges from 9.42 MPa to 34.8 MPa, with an average modulus of 16.3 MPa [28]. Since the designed mesh will primarily interact with this bone segment, an elastic modulus of 16.3 MPa or lower is preferred. Another mechanical property which is to be considered involves the yield stress. The yield stress will determine the stress level at which the material will yield and plastically deform, ensuring the material retains the imposed shape. To imitate the mechanical properties of the surrounding bone tissue in a Paprosky 3A situation a yield stress of 0.64 MPa or lower is required [28]. While meeting these mechanical conditions is essential, maintaining the structural integrity of the mesh is most crucial. Complete detachment of struts poses a serious safety hazard and could resolve in severe complications. Therefore complete detachment of struts is an unacceptable result given any particular design.

The second domain of functional requirements involves insertion. The designed mesh will be inserted by a surgeon through impactation, and must therefore withstand the corresponding (changing) conditions. This includes the use of a standard 700-gram orthopedic mallet. The application of such a mallet by surgeons results in an average of 8.81 Joules of kinetic energy per strike [32]. Given these conditions, peak forces below 8.9 kN are to be expected [33]. Higher peak will make damaged bone tissue most probable. The peak forces provide localized concentration of high stresses and must therefore be considered in the design. Given the before mentioned conditions, the mesh must adapt to the shape of the Paprosky 3A defect without losing the structural integrity of the mesh.

The third domain evaluates the potential biocompatibility of the design. Whether the material allows the ingrowth of tissue is affected by the available surface area. A higher surface area allows tissue to easily attach itself, yet enough space must be available to provide clear entrance to the deeper layers of the lattice structure. Taking this into account, literature suggest a pore size ranging from 50 µm to 800 µm is ideal [15]. The material used has a significant effect on the biocompatibility of a medical implant. An implant must ensure low reactivity with the surrounding tissue to prevent any safety hazards. Titanium alloys are commonly used due to several key characteristics. The most crucial characteristic is the corrosion resistance. As titanium forms a protective oxide layer on it's surface when exposed to air or moisture, any chance of an immune response remains unlikely [34].

The last domain contains the production of the design. Given the micro-structure of the designed lattices, small irregularities in the final design significantly affect the mechanical characteristics, providing uncertainties in the designed properties. These irregularities, resulting from the SLM manufacturing technique, include inconsistencies in the cross-sectional area of the struts and imperfect fusion of powder particles[22]. Thicker struts, with a larger cross-sectional area, are more capable in withstanding thermal stresses and laser-induced forces. The SLM machine used and provided by AMNOVIS has a printing accuracy of up to 200 µm. To prevent possible irregularities, the cross-sectional area was enlarged by establishing a strut thickness of 300 µm.

Requirement ID	Requirement Definition	Demand/Wish
1. Mechanical Properties		
1.1.	The elastic modulus is within 0.83 MPa and 89 MPa [28]	Demand
1.2.	The elastic modulus is below 16.3 MPa[28]	*Wish*
1.3.	The compressive yield stress is below 0.64 MPa [28]	*Wish*
1.4.	There is an absence of total strut fractures	Demand
2. Insertion		
2.1.	The material should be adabtable to the shape of a Paprosky 3A defect	Demand
2.2.	The impactation tests should simulate the case of a common 700 g orthopedic mallet during revision THA	Demand
2.3.	The material must be able to deform within the force applied by surgeons during (revision) THA surgeries, given 8.81 Joules of kinetic energy[32]	Demand
2.4.	The impact forces remain below 8.9 kN [33]	Demand
2.5.	Following the surgeon's insertion of the mesh into a Paprosky 3A Acetabulum, all areas of bone resorption are filled	*Wish*
3. Biocompatibility		
3.1.	The pore size is between 50 µm and 800 µm [15]	Demand
3.2.	The used material is pure titanium, or a titanium alloy	Demand
3.3.	The used material is CP-Ti grade 1 [34]	*Wish*
4. Production		
4.1.	The strut thickness is set to 300 µm	Demand
4.2.	The material is designed through the use of a lattice strut model	Demand

Table 1: Requirements according to the Functional Requirement Analysis model

2 Selection of Mesh Design and Methodology

2.1 Selection of Mesh Design

2.1.1 Material Selection

The use of pure titanium or a titanium alloy is required. However, to seize improved biocompatibility, commercially-pure-titanium (CP-Ti) grade 1 was applied, as preferred according the defined requirements, see table 1.

2.1.2 Lattice Design Selection

To guarantee a low level of uncertainty in the design of the material properties, a non-stochastic lattice was employed. The ideal mesh requires a low stiffness-, but high strength complex. Thus the design space was limited to non-auxetic lattice structures. Given the selected material is CP-Ti grade 1, chapter 2.1.1, the manufacturing method involves SLM. Consequently, a surface-based lattice is rejected and a strut-based lattice is implemented in the design.

The choice of a lattice unit cell remains challenging. Much research has been conducted given single type of unit cells, while comparative information remains scarce. The BCC-, and diamond unit cells are frequently applied due to a high strength-to-weight ratio, facilitating a load bearing function while reducing the chance of fatigue and discomfort [25]. To answer the before mentioned research question, see chapter 1.2.1, both BCC- and diamond unit cells will be included in designing a deformable titanium lattice mesh.

The different unit cell types this study will include are three BCC based-, and three Diamond based lattice samples, composed of SLM printed CP-Ti grade 1. Each sample will be a cube with an equal length, width and depth of 41,6 mm.

To compare both lattice types, the length/thickness strut ratio will be varied to 5, 10 and 15, given a constant strut thickness of 0.3 mm and an appropriate unit cell size. The details given the different lattice structure designs are provided in table 2. The formula used to modify the dimensions of the Diamond lattice structure, equation 1, are obtained from Ahmadi et al. [35]. The calculations involving the length and the fitting dimensions of the unit cell size concerning the BCC unit cell type, equation 2, are based on the formula provided by Magré et al [36]. Figure 5 presents all sample types before testing.

Diamond					
	Ratio	Strut Thickness (mm)	Strut Length (mm)	Unit Cell Size X,Y,Z (mm)	Sample Size X,Y,Z (mm)
	5	0.3	1.5	3.5	41.6
	10	0.3	3	6.9	41.6
	15	0.3	4.5	10.4	41.6
BCC					
	Ratio	Strut Thickness (mm)	Strut Length (mm)	Unit Cell Size X,Y,Z (mm)	Sample Size X,Y,Z (mm)
	5	0.3	1.5	1.7	41.6
	10	0.3	3	3.5	41.6
	15	0.3	4.5	5.2	41.6

Table 2: Diamond and BCC Sample Specifications

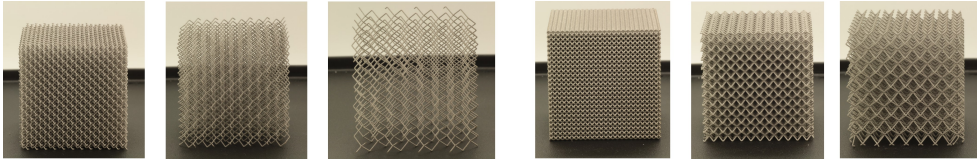

Figure 5: Sample types from Left to Right - Diamond Ratio: 5/10/15 & BCC Ratio 5/10/15

2.2 Methodology

To answer the main research question, see chapter 1.2.1, all 3 main sub-questions are addressed. Given all 3 main sub-questions require the use of micro-CT scans, the general approach of conducting such scans is dictated below:

Micro-CT Scan

To evaluate the complete disengagement of struts during the uniaxial drop test and the uniaxial compression test, visual inspection and the analysis of Micro-CT scans have been applied. Determining the potential of osseointegration required the use of Micro-CT scans as well. The additional use and processing of the Micro-CT scans is defined in chapter 2.2.3. In conducting Micro-CT scans, the Quantum FX µCT machine located at UMC Utrecht was employed, see figure 6. The acquired scans have been saved as DICOM files and processed using the Mimics software [37]. Using the processed files any complete disengagement of struts could be analysed.

Figure 6: Quantum FX µCT machine

2.2.1 Material Response to Uniaxial Impact

Uniaxial Drop Test

To answer the research sub-question 1, the Dynatup 8250 was employed. The Dynatup 8250 machine was deployed to execute the uniaxial drop test, see figure 7. All samples have been centrally positioned on the bottom plate of the Dynatup 8250 machine. To ensure uniform distribution a metallic plate was positioned on top of all samples given a width and length of 45 mm. A value of 8.81 joules kinetic energy is applied during a singular strike by a surgeon [32]. According equation 4 this implies the use of a 2.64 kg load cell at a height of 0.34 m. The Dynatup 8250 machine made use of the Kistler 9011A sensor. The electrical charges produced by this sensor have been amplified using the Kistler type 5011, and used to determine the dynamic forces and displacement during impact. Applying the obtained data, force-displacement curves of all samples were gathered. By using these curves, the elastic strain of each curve was captured according ISO standard 2439 [38], requiring the division of the difference in top- and ending displacement of the curve with the total height of the sample. The obtained data was analyzed using the One-Way ANOVA method. Results were considered statistical significant given $p < 0.05$, to answer sub-question 1.

Figure 7: Uniaxial Drop Test Setup

2.2.2 Material Response to Uniaxial Static Compression

Uniaxial Static Compression Test

In answering subquestion 2 an uniaxial static compression test, and a digitial camera system, was employed. During the uniaxial static compression test the ARAMIS v6 system and Zwick/Roell Z5.0 machine were utilized.

To answer question 2.2.1 a digital camera system, called the ARAMIS v6 system was deployed. The ARAMIS v6 system uses an optical technique to measure deformation and strain of a sample's surface before, during and after loading. The surface structure is recognized and measured through utilizing two 12 Megapixel digital cameras, at a camera angle of 25°, from a measuring distance of 0.45 m, see figure 8. Before testing all samples are spray painted with graphite to provide a random speckled pattern on the sample's surface. By using the 12 Megapixel digital cameras, the ARAMIS allocated the coordinates of the speckles in a 3x3 unit cell array throughout the compression test. Using the obtained data, lateral and axial strain, during the compression of the 3x3 unit cell array, was determined, see figure 9. With this information a graph containing a lateral- and axial strain ratio with respect to lateral strain was established.

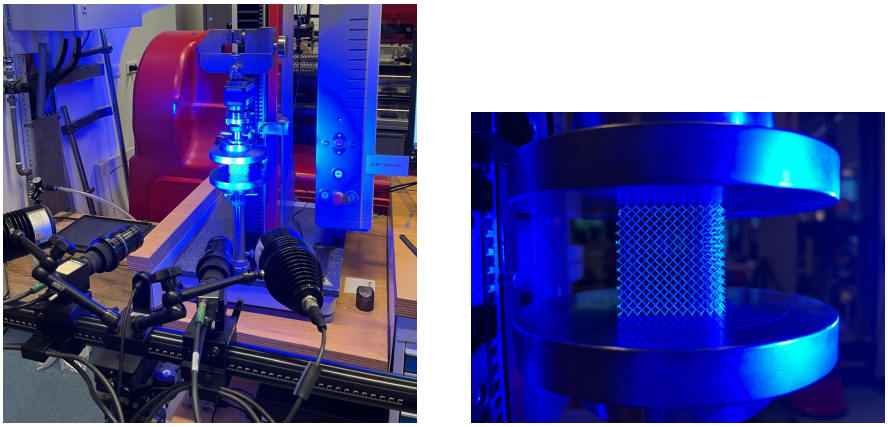

(a) ARAMIS Camera Setup (b) ARAMIS Sample Setup

Figure 8: ARAMIS Setup

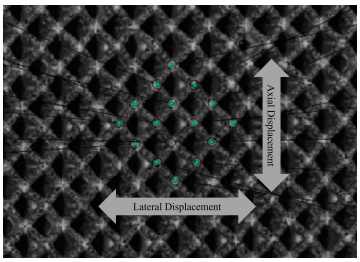

Figure 9: Interpretation Axial-, and lateral Displacement of a 3x3 Unit Cell Array

Addressing question 2.2.2 was facilitated by the Zwick/Roell Z5.0 machine according ISO standard 13314 [39]. A load of 5 kN was applied with a constant deformation speed of 2 mm/min until a force of 5kN was reached or fractures in the sample were observed.

The force-displacement curves gathered by the Zwick/Roell Z5.0 machine were used to acquire the stress-strain curves. The required stress values were obtained by the division of the applied force with the initial cross-sectional area of 1730.56 mm^2. The strain was determined by dividing the axial displacement with the initial height of 41.6 mm. The elastic modulus was calculated by the appliance of equation 3 in the elastic region of the stress-strain curve. To determine the yield stress the 0.2% offset method was employed in accordance with ISO standard 13314 [39]. The extent of the plateau stress was also measured according ISO standard 13314 [39]. To determine the start of the plateau, the average stress in the interval of 20% and 40% strain is to be calculated. When the elastic region has ended and the average plateau stress is attained by the stress-strain curve, the given strain is defined as the starting point of the plateau stress. According ISO standard 13314 [39], the end of the plateau is reached when the curve crosses a stress 1,3 times higher than the calculated average plateau stress. The difference in strain between the start- and end point of the plateau is interpreted as the average plateau size. The statistical One-Way ANOVA method was applied to analyze the elastic modulus and yield stress given the corresponding length/thickness strut ratio. Results were considered statistical significant given $p < 0.05$.

2.2.3 Potential of Osseointegration

Material Property Comparison of Mesh and Bone Tissue

To determine the potential of osseointegratioin, see sub-question 3, the extent of mimicking surrounding bone tissue is determined to answer sub-question 3.1 by using results attained in chapter 3.2.2. The degree of mimicking surrounding bone tissue is measured by comparing the elastic modulus and yield stress with respect to the properties of surrounding bone tissue defined in table 1.

Mesh Morphology

In answering sub-question 3.2, the potential of bone ingrowth is determined through the measurement of the pore sizes before and after uniaxial static and impact compression. This measurement was executed by the use of the previously mentioned Micro-CT procedure. Additionally, the software 3-matic [40] was utilized. Using this software, the Micro-CT scans were converted into 3D meshes. The meshes were optimized to be transformed into volume meshes. With the use of the volume meshes, the software was enabled to determine the average pore size before and after compression. The pore sizes were defined as the radius of a sphere located in the center of a pore, see figure 10. Given the changes in morphology, both Micro-CT scans and the converted 3D models were used to recognize changes in the design- and pore morphology. These developments were not quantified but merely described based on visual observation.

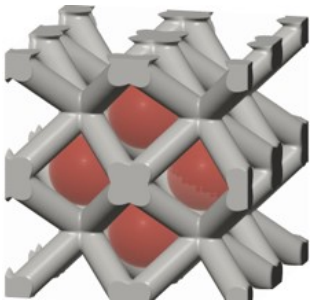

Figure 10: Pore Size Definition

3 Results

3.1 Results Material Response to Uniaxial Impact

3.1.1 Results: Micro-CT Scan

After the execution of the uniaxial drop test, no complete disengaged struts were identified through visually observations or analysis of Micro-CT scans.

The degree to which the lattice constructs adapted itself to a singular impact strike differed as displayed by the Micro-CT scans in figure 11 and 12. The BCC based designs show limited vertical displacement in contrast to diamond based designs. Moreover, BCC based designs did not show signs of buckling struts but presented global buckling at a ratio of 15. Diamond based designs did show signs of buckling struts at a ratio of 10 and 15. Global buckling was also observed in diamond based meshes containing a ratio of 10.

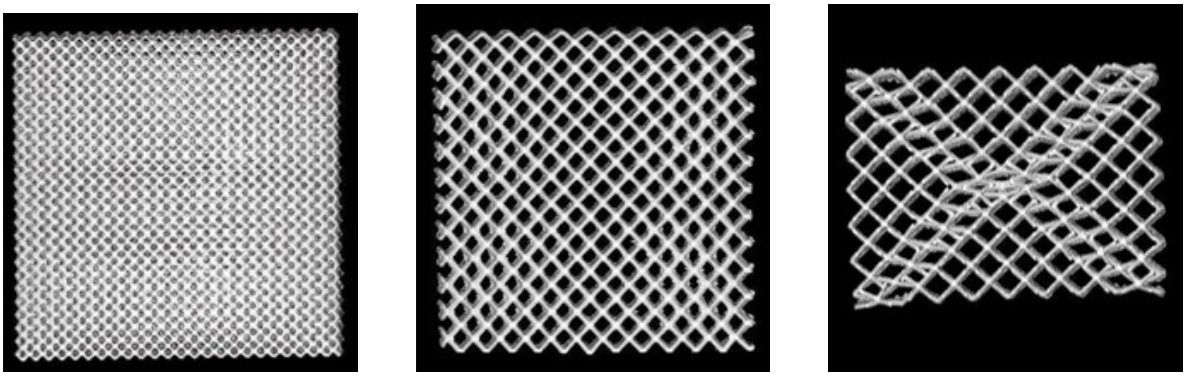

(a) BCC Ratio 5 (b) BCC Ratio 10 (c) BCC Ratio 15

Figure 11: Micro-CT scans of BCC Unit Cell Types after Impact

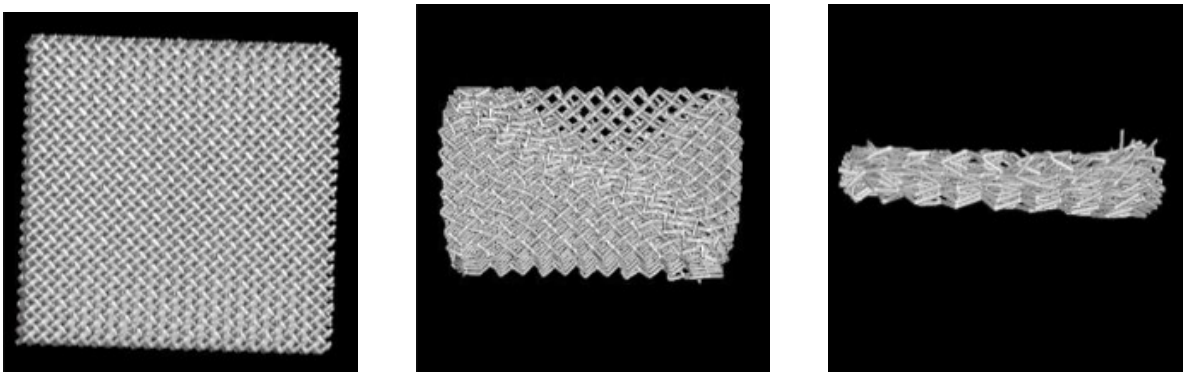

(a) Diamond Ratio 5 (b) Diamond Ratio 10 (c) Diamond Ratio 15

Figure 12: Micro-CT scans of Diamond Unit Cell Types after Impact

3.1.2 Results: Uniaxial Drop Test

Peak Forces

Using the force-displacement curves, shown in Table 3, the maximum peak forces remained below the maximum value of 8.9 kN. The BCC-based designs showed higher peak forces in respect to diamond-based designs. Moreover, the BCC samples showed a steep decline in peak force as the length/thickness ratio increased. The diamond designs showed a less steep decline in peak force.

Ratio	Diamond	BCC
5	3442	7598
10	1109	2400
15	912	1135

Table 3: Impact Peak Forces (N)

Elastic Strain

The force-displacement curves provided understanding in the developing elastic strain of the different designed meshes, see figure 13. All samples showed an elastic strain below 9%, conforming the prominent extent of plastic deformation and the small degree of elasticity. The diamond unit cell types showed a linear decline in elastic strain,($p < 0,05$), given a proceeding length/thickness ratio. Nevertheless, the BCC unit cell types demonstrated an opposite linear increase in elastic strain, ($p < 0,05$), given an advancing length/thickness ratio.

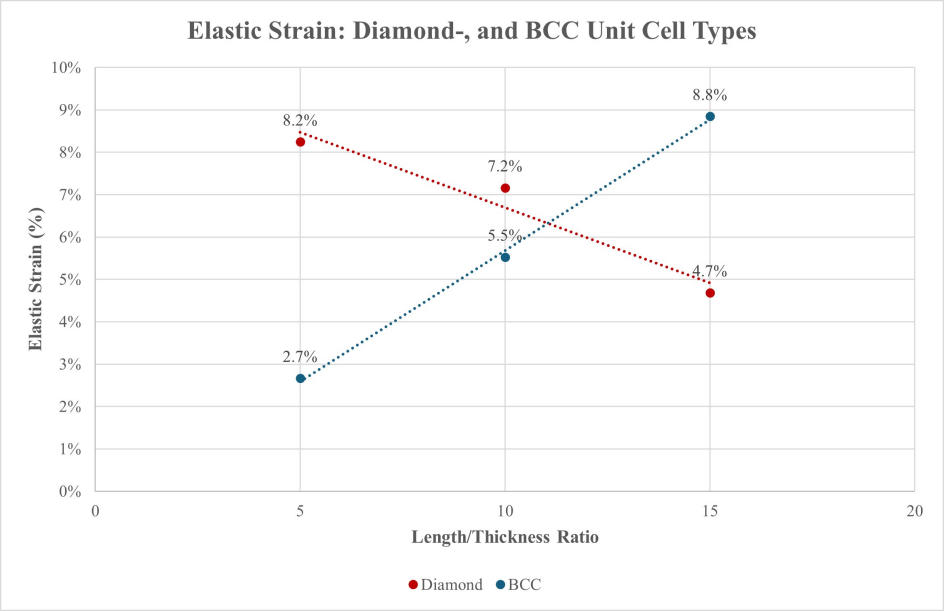

Figure 13: Average Elastic Strain given a proceeding Length/Thickness Ratio

3.2 Results Material Response to Uniaxial Static Compression

3.2.1 Results: Micro-CT Scan

After uniaxial static compression, no complete disengagement of struts was identified through the appliance of executing Micro-CT scans and visual inspections.

Similar to the results of chapter 3.1.1, the BCC based meshes showed modest vertical deformation in respect to the fast vertical displacement of diamond based meshes. The BCC designs display a clear layer-by-layer collapse through an increasing ratio while no local- or global buckling is established. Furthermore, diamond based samples show distinct signs of local- and global buckling at a ratio of 5. Moreover, these designs show the appearance of bulging. At a ratio of 10 and 15 all diamond based samples have achieved near full vertical compression. Additionally, the diamond samples demonstrate indications of a layer-by-layer compression at a ratio of 10 and 15.

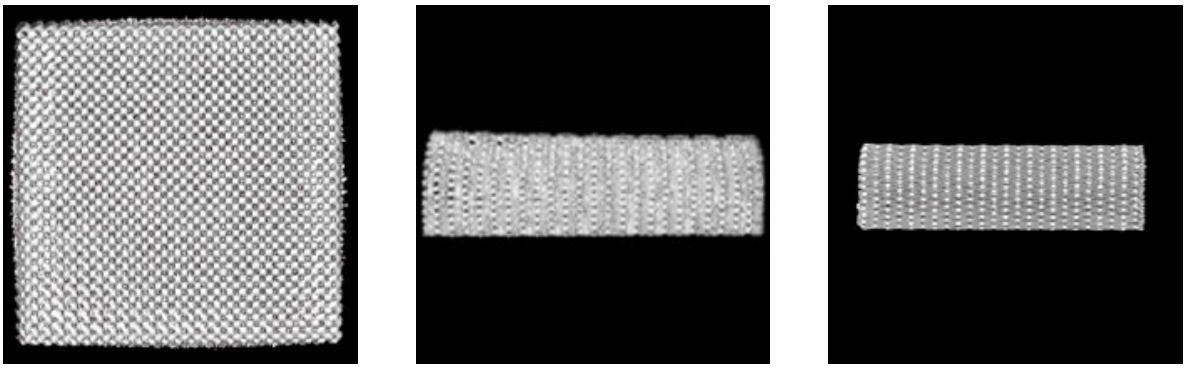

(a) BCC Ratio 5 (b) BCC Ratio 10 (c) BCC Ratio 15

Figure 14: Micro-CT scans of BCC Unit Cell Types after Uniaxial Static Compression

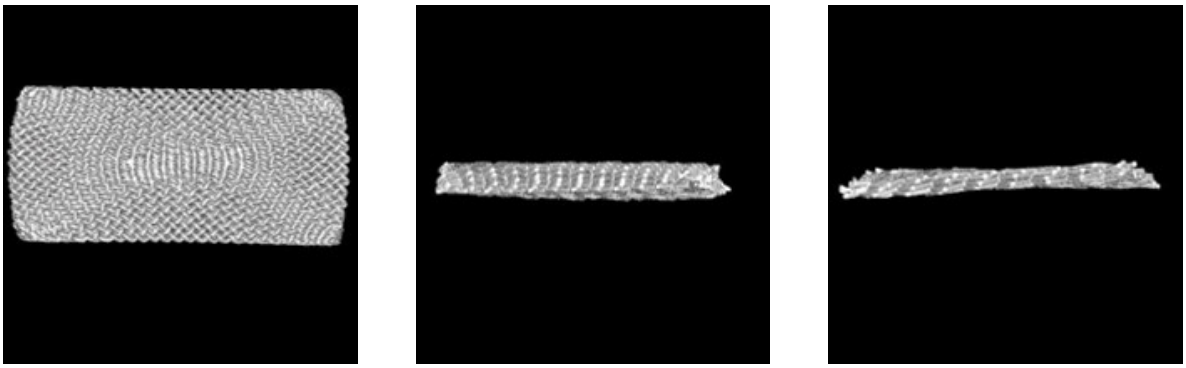

(a) Diamond Ratio 5 (b) Diamond Ratio 10 (c) Diamond Ratio 15

Figure 15: Micro-CT scans of Diamond Unit Cell Types after Uniaxial Compression

3.2.2 Results: Uniaxial Static Compression Test

-Lateral Strain(LS)/Axial Strain(AS) Ratio

Figure 16 shows a change in the -LS/AS ratio given a developing AS. The diamond based construct with a ratio of 5 displays high -LS/AS ratios in respect to other designs. Furthermore, the declining -LS/AS ratio persists through a developing axial strain. Moreover, the BCC samples with a ratio of 10 and 15 show a similar trend given a lower developed strain. Diamond meshes containing a ratio of 10 and 15 attain lower -LS/AS ratios and fail given smaller strain values.

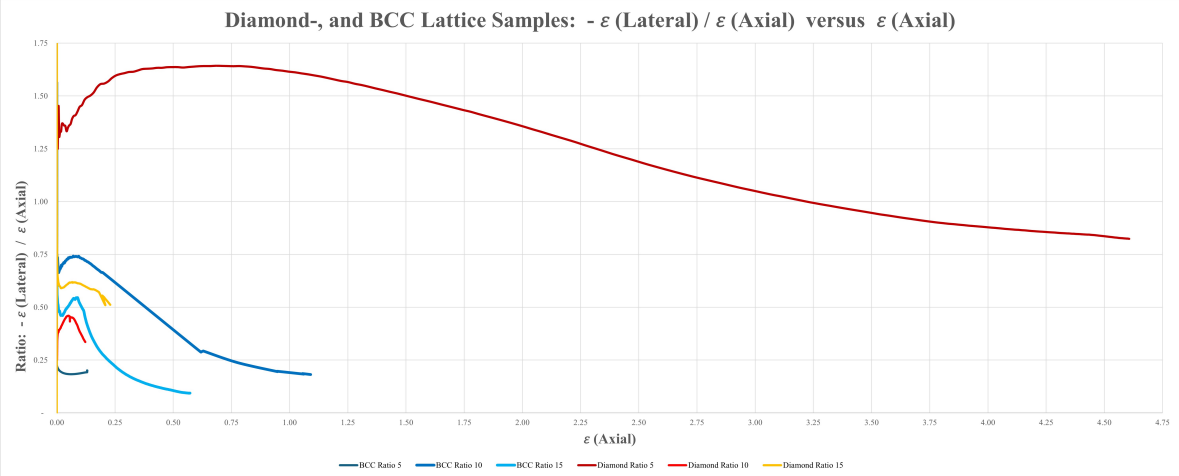

Figure 16: The Lateral Strain/Axial Strain Ratio with respect to Axial Strain

Stress-Strain Curves

As depicted in figure 17, the stress-strain curves show distinct differences in material performance. Throughout the analysis, sample 24, a BCC ratio 5 design, was excluded in all calculations to maintain accordance with ISO standard 13314 [39]. The BCC designs with a ratio of 5 were discarded in the calculation of the yield stresses. This was due to the unyielding of the samples.

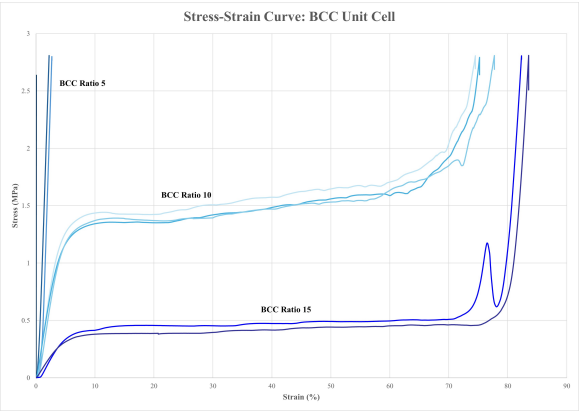

(a) Stress-Strain Curves BCC

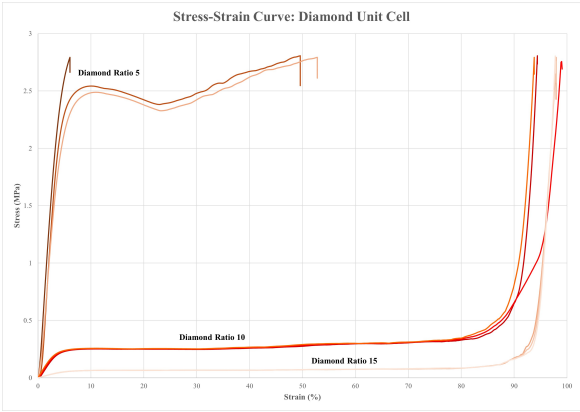

(b) Stress-Strain Curves Diamond

Figure 17: Overall caption for the figures

Elastic Modulus

The elastic moduli depicted in figure 18, expose an exponential correlation with respect to the length/thickness ratio (Diamond: $p < 0.001$; BCC: $p < 0.001$). The BCC ratio 5 sample 24 was excluded due to measurement complications. Given the functional requirements outlined in table 1, all designs, except the BCC ratio 5 structure, exhibited an elastic moduli in a range of 0.83 MPa and 89 MPa. The wish of an elastic modulus below 16.3 MPa is met by the BCC ratio 15 design, and diamond constructs possessing ratios of 10 and 15.

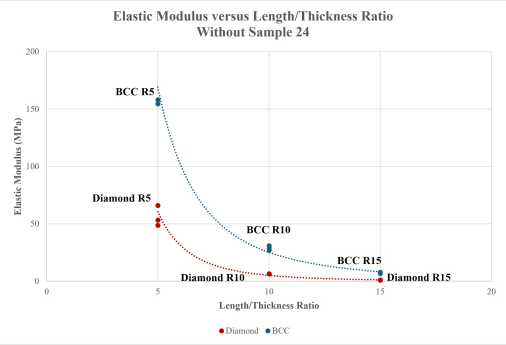

Figure 18: Elastic Moduli of Diamond- and BCC unit cell designs

Yield Stress

The diamond yield stresses showed a statistical significant exponential correlation ($p < 0.002$). The functional requirements dictate a yield stress below 0.64 MPa. The BCC design with a ratio of 15, and the diamond design with a ratio of 10 and 15 are in accordance with this requirement.

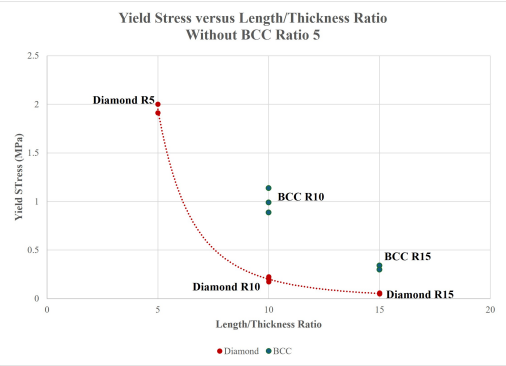

Figure 19: Yield Stresses of Diamond- and BCC unit cell designs

Plateau Stresses

All unit cell designs, except the BCC ratio 5 design, achieved plastic deformation, differing in point of plastic deformation and size. As depicted in figure 17, diamond lattice structures plastically deform at lower levels of stress relative to BCC lattice structures. The average plateau sizes are provided in table 4. The diamond lattice designs show higher plateau sizes with respect to the BCC lattice designs.

Ratio	Diamond	BCC
5	51.2%	no plateau
10	75.2%	65.3%
15	75.3%	70.7%

Table 4: Average Plateau Size

3.3 Results of Potential Osseointegration

3.3.1 Results: Material Property Comparison of Mesh and Bone Tissue

Elastic Modulus

The elastic modulus is required to be in between 0.83 MPa and 89 MPa. To be most similar with the surrounding bone tissue an elastic modulus below 16.3 MPa is preferred, see chapter 1.2.2. The diamond-based designs with a ratio of 10 and 15, with the additional BCC-based design containing a ratio of 15, are in line with this wish.

Yield Stress

The yield stresses are to be below a value of 0.64 MPa; see chapter 1.2.2. The diamond-based designs given a ratio of 10 and 15, accompanied by a BCC design including a ratio of 15, meet this requirement.

Design Space: Elastic Modulus and Yield Stress

Figure 20 displays a representation of the requirements/wishes of the elastic moduli and yield stresses. The red lines describe the limit of values, green boxes represent the available design spaces. Figure 20 shows BCC designs with a ratio of 15, and diamond based designs with a ratio of 10 and 15 to be within the required design space, and comply with the design wishes.

Figure 20: Available Design Space

3.3.2 Results: Mesh Morphology

Resulting Pore Sizes of Impact Uniaxial Compression

The resulting pore sizes after the uniaxial drop test display high variation in the resulting pore sizes, see table 5. All designs, with the exception of the BCC designs having a ratio of 15, suffice to the previously defined requirements, see table 1.

Ratio	Diamond	BCC
5	0.32	0.33
10	0.60	0.77
15	0.69	1.16

Table 5: Pore Size after Uniaxial Impact (mm)

The relative change in pore size differs significantly also, see table 6. While the diamond-based samples display high levels of decline in pore size, BCC-based samples reveal minimal change. Worthy of notion is the difference in the evolving decline of pore size. While the diamond-based constructs portray a gradual increase in pore size decline, the BCC-based designs portray a swift decline.

Ratio	Diamond	BCC
5	67%	3%
10	74%	4%
15	82%	13%

Table 6: Decline in Pore Size after Uniaxial Impact

Resulting Morphology of Impact Uniaxial Compression

The BCC designs, see figures 21, 22, 23, show modest change in vertical shift throughout a proceeding length/thickness ratio. While the BCC designs at a ratio of 5 demonstrate minimal deviation in pore size and vertical displacement, significant changes in morphology of the BCC designs emerge at a ratio of 15. The side view shows clear signs of lateral expansion, while the top view reveals slight contraction in the coronal direction. The side view also distinctly displays the global buckling effect. The global buckling effect also explains why the lateral side segments from a top view are more dense. This significant difference in resulting pore sizes are supported by table 5, as well.

The morphology of pores in the BCC models seems to endure minimal change. The non-stochastic pattern remains and only deviates at a ratio of 15. At a ratio of 15 the global buckling effect changes the morphology of pores. As seen in figure 23, different segments start to flatten, while spaces in between appear stretched.

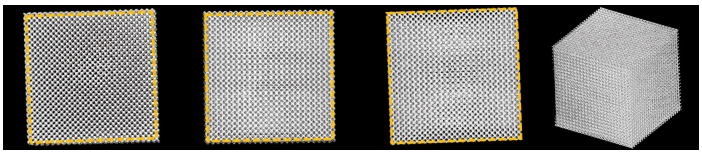

Figure 21: BCC Ratio 5: Frontal-, Side-, Top-, and Isotropic View

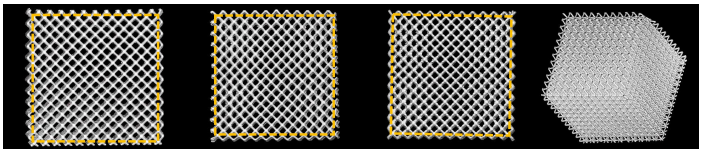

Figure 22: BCC Ratio 10: Frontal-, Side-, Top-, and Isotropic View

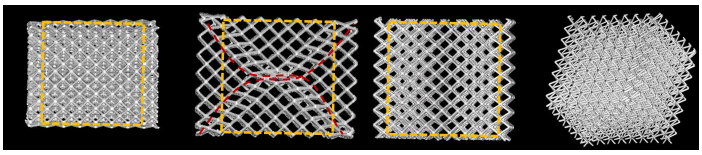

Figure 23: BCC Ratio 15: Frontal-, Side-, Top-, and Isotropic View

The diamond designs, see figures 24, 25, 26, present an initial dense material at a ratio of 5 also. However, when a ratio of 10 is attained, global buckling occurs. Moreover, local buckling enforces the transformation of a non-stochastic structure towards a stochastic architecture. Just like the BCC samples with a ratio of 15, see figure 23, the samples transforms into a rectangular structure through lateral expansion and coronal contraction. Additionally, while the diamond ratio 10 samples are transforming into a rectangular configuration and endure the global- and local buckling effect, the lateral expansion displays bulging as well. At a ratio of 15 the diamond samples have been vertically compressed to such an extent that the identification of global buckling or bulging is not applicable. However, the rectangular transformation is still recognized.

Distinct changes in pore size morphology of diamond based samples are observed at a ratio of 10 and 15. Just like the BCC based samples at a ratio of 15, see figure 23, the global buckling enforces the contraction and stretching of pores. The decline in pore size alone can not be explained through the global buckling alone. As the global buckling enforces flattening of the pores, the more extensive vertical compression has been recognized to impose local buckling. At a ratio of 15, the diamond based samples have lost the structural integrity due to local buckling and have withstood near full vertical compression.

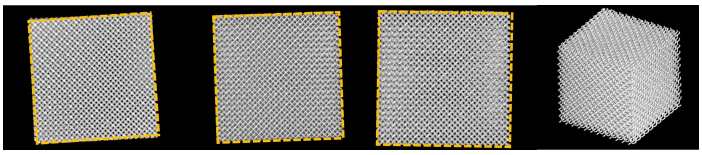

Figure 24: Diamond Ratio 5: Frontal-, Side-, Top-, and Isotropic View

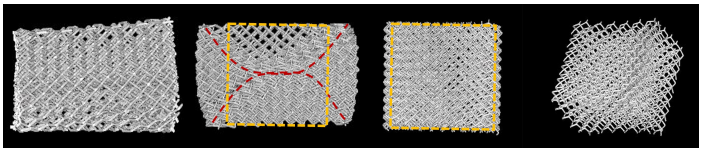

Figure 25: Diamond Ratio 10: Frontal-, Side-, Top-, and Isotropic View

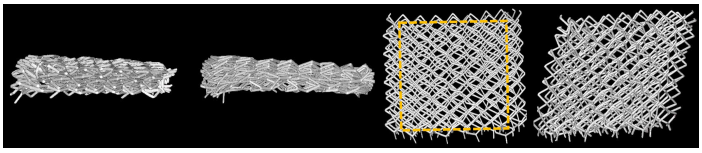

Figure 26: Diamond Ratio 15: Frontal-, Side-, Top-, and Isotropic View

Resulting Pore Sizes of Static Uniaxial Compression

All final pore sizes are shown in table 7. In accordance with the functional requirements, see table 1, a pore size in between 0.05 mm and 0.8 mm is prescribed. All samples fit this necessity. Moreover, the final pore sizes are similar in value for all designs, with the exception of the BCC based design featuring a length/thickness ratio of 10.

Ratio	Diamond	BCC
5	0.35	0.30
10	0.31	0.65
15	0.36	0.30

Table 7: Pore Size after Uniaxial Static Compression (mm)

The resulting pore sizes remain similar given the different designs. An exception is the BCC construct with a ratio of 10. Nonetheless, the different designs show distinct differences in the relative decline in pore size, see table 8. The diamond based designs show a strong decline in pore size, which gradually increases over an increasing ratio. The BCC based meshes present a smaller decline in pore size but display a sudden increase at a ratio of 15.

Ratio	Diamond	BCC
5	64%	10%
10	86%	19%
15	91%	34%

Table 8: Decline in Pore Size after Uniaxial Static Compression

Resulting Morphology of Static Uniaxial Compression

The Micro-CT scans of BCC based designs, show initially minimal deformation, see figure 27. Through the use of yellow squares as point of reference, a proceeding length/thickness ratio causes lateral expansion and coronal contraction, see figures 28 and 29. A slight bulging effect is observed in uniaxial statically compressed BCC samples. However, the degree of bulging is interpreted as less significant. Unlike the diamond samples at a ratio of 10 and 15 which endured impact, the uniaxially static compressed BCC samples maintain a non-stochastic without the incidence of the global buckling effect.

Throughout this transformation of the BCC based samples, the struts are pressed against each other forming "walls". While lateral expansion and coronal contraction occurs, the non-stochastic structure remains due to a layer-by-layer collapse. Deviations are to be found in the horizontal and vertical dimension of the pores, but the rectangular morphology remains.

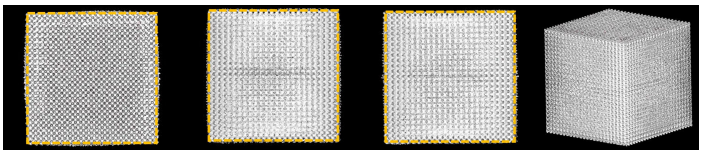

Figure 27: BCC Ratio 5: Frontal-, Side-, Top- and Isotropic View

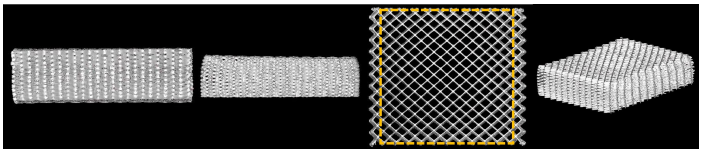

Figure 28: BCC Ratio 10: Frontal-, Side-, Top- and Isotropic View

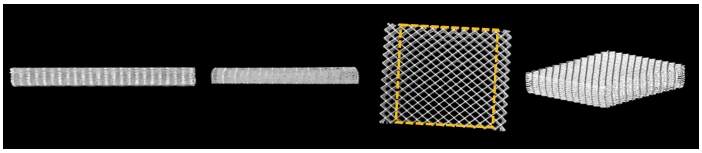

Figure 29: BCC Ratio 15: Frontal-, Side-, Top- and Isotropic View

The Micro-CT scans after uniaxial compression of the diamond based meshes, see figures 30, 31 and 32, show distinct differences in it's response to uniaxial static compressed BCC based samples. As displayed in figure 30, the occurrence of global buckling in diamond based samples involving a ratio of 5 is evident. Also, the transformation of lateral expansion and coronal contraction are displayed in all diamond samples. Moreover, the bulging of samples is most prominent in diamond samples containing a ratio of 5.

A stochastic structure is identified in all uniaxial static compressed diamond based meshes. A notion is made concerning the visually observed densifying of pores. An observation supported by the results in table 8. Given the length/thickness ratio's of 10 and 15, the samples have provided near vertical compression. In this instance the struts present buckling of struts and a consecutive deviation in pore morphology.

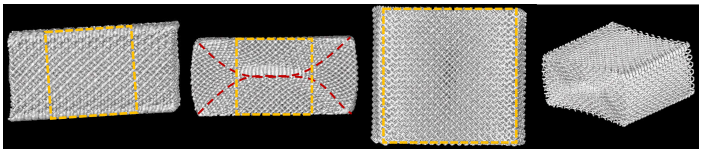

Figure 30: Diamond Ratio 5: Frontal-, Side-, Top- and Isotropic View

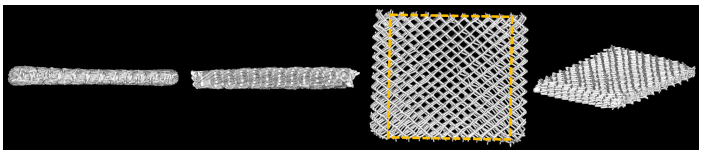

Figure 31: Diamond Ratio 10: Frontal-, Side-, Top- and Isotropic View

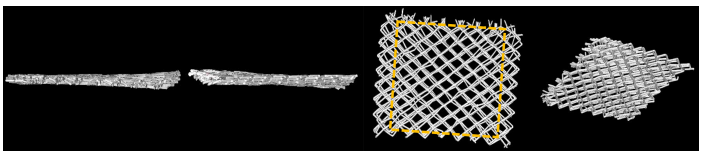

Figure 32: Diamond Ratio 15: Frontal-, Side-, Top- and Isotropic View

4 Discussion

4.1 Discussion about the Material Response to Uniaxial Impact

The results of the Micro-CT scans showed no signs of complete disengaging struts, see chapter 3.1.1, and therefore answered research question 1.1. The promise of no disengaged struts after impact, given the predefined conditions in chapter 2.2.1, presents the potential of applying lattice meshes in Paprosky 3A defects without causing safety hazards.

How the material will give in to a simulated singular strike, research question 1.2.1, proved to differ for the considered designs. Figure 13 displayed these differences and revealed diamond based meshes to develop a linear decline in elastic strain considering an evolving length/thickness strut ratio. The BCC samples showed an opposite trend, presenting a linear increase in elastic strain when considering a growing length/thickness strut ratio. The differences in morphology, presented in chapter 3.3.2, clarifies these different trends. The BCC based designs show negligible/modest buckling of struts, while ratio 10- and 15 diamond based designs present prominent global- and local buckling. The difference between these meshes is the vertical collapse. The yielding of struts and consecutive collapse of the different layers, resulted in a near fully compressed sample at a ratio of 15. The BCC samples with similar ratios showed minimal vertical deformation. Moreover, these BCC designs showed little signs of buckling struts. The observations of a growing elastic strain and lack of buckling struts in BCC based designs during the exposure to dynamic forces is confirmed by literature [41]. This indicates that BCC samples are able to withstand the impacted load, while the more rigid diamond lattice structure can not and consecutively provide a quick collapse of the design when a unit cell fails [21, 42]. The failing of diamond struts in bearing the impacted load unfolded in plastic deformation. Due to the BCC designs being able to withstand this dynamic load and the increase in slenderness of struts attributed to an increasing length/thickness ratio, clarified the increase in elastic strain. The diamond meshes at a ratio of 10 and 15 were not able to withstand the impacted force, clarifying the decline in elastic strain.

The increasing elastic strain off BCC based samples will offer the surgeon more flexibility in the impactation process of the material. However, in the tested samples elastic strains remained below 9%, thus pursuing a high degree of plastic deformation. Furthermore, the peak forces of BCC based designs, although they are within the allowed range of values defined by requirement 2.4, are considered steep, see table 3. Specifically, the BCC based designs involving a ratio of 5 displays substantial peak forces. High peak forces may enforce high stresses on weakened bone tissue resulting in damaged bone tissue. There is no direct correlation of peak forces in respect towards the elastic modulus, damping and energy absorption. How these variables can be applied in the prediction of resultant peak forces is to be established in future research. The preferred degree of elastic strain will have to be examined in collaboration with orthopaedic surgeons. Using BCC samples with higher ratios could help in designing such strains.

Addressed by research quesion 1.2.2, the different designs showed variations in their response to impact. Through an increasing ratio, the BCC based designs maintained a non-stochastic architecture. The diamond samples display a different response by revealing a stochastic structure of buckling struts at a ratio of 10, evolving into near complete vertical compression of diamond samples at a ratio of 15.

In response to research question 1, the expected behaviour of the tested meshes, when impacted by a surgeon in a Paprosky 3A situation, involves struts having kept attached to the lattice structure. BCC samples with a higher ratio are expected to provide the surgeon more flexibility in the insertion process, thus showing more potential in respect to diamond based constructs. However, future research will be required to confirm this assumption and determine a most beneficial elastic strain value. Furthermore, BCC based meshes will be able to pursue a non-stochastic pattern during impact, given an increasing ratio in contrast to diamond based meshes.

4.2 Discussion about the Material Response to Uniaxial Static Compression

In executing the uniaxial static compression test, no disengaged struts were observed, thus resolving research question 2.1. This provides confidence in BCC- and diamond titanium based meshes to counter potential safety hazards when statically compressed by orthopaedic surgeons.

The uniaxial static compressed smaples displayed a difference in response, see figure 16. The diamond meshes with a ratio of 5 provided the highest -LS/AS ratios. The design was also able to maintain lateral expansion throughout a considerable axial strain. As shown in the final morphology of the sample, see figure 30, the design was able to refrain struts from yielding and showed significant bulging through the global buckling of the mesh. The yield stresses of this particular design, see figure 19, are high due to the exponential relationship of yield stress and the length/thickness ratio. Given the lower yield stresses of additional diamond designs, struts failed in their load bearing function hence a collapse of the different layers established plastic deformation and limited a development of the -LS/AS ratio. The BCC designs provided modest -LS/AS ratios in respect to the diamond ratio 5 design. However, the BCC designs with a ratio of 10 and 15 pursued considerate lateral expansion given a proceeding axial strain compared to similar diamond derived designs. However, due to high yield stresses buckling was resisted and the extent of lateral expansion was limited. Enhancing lateral expansion in BCC designs could be attained by modifying the yield stress of the material. Deploying higher length/thickness strut ratios or post-processing methods as Hot Isostatic Pressing (HIP) [43, 44], will lower the yield stress and contribute to such design. In answering research question 2.2.1, a higher yield stress and low length/thickness ratio is expected in enabling diamond based designs to provide significant lateral expansion. BCC based samples will require higher ratios and/or post processing methods such as HIP to ensure lower yield stresses, to attain enhanced lateral expansion when subjected to static compression in a Paprosky 3A defect.

The design challenge of ensuring the seating of the material, was addressed by research question 2.2. The BCC samples proved to plastically deform at higher levels of stress relative to the diamond based designs, see figures 17a and 17b. The diamond designs established longer plateau sizes, see table 4. In the context of a THA procedure, a long plateau would indicate the designed material is seating within the particular defect. Given this statement a diamond based design would be most promising. However, as the diamond based designs with a ratio of 10 and 15 illustrate, these designs plastically deform at low levels of stress. Consequently the surgeon has limited flexibility in properly shaping the designed material. The early occurrence of plastic deformation is assumed to be even more prominent in a real THA procedure. While the samples in this research are compressed without being enclosed, this will not be the case when inserted in a Paprosky 3A defect. The compression of a mesh in a confined environment will enforce high stresses from all directions. While surrounding fractures will be filled through lateral expansion, the available directions are limited. The higher stresses will ensure the collapse of layers, enhancing the stiffness of the mesh [15, 45].

The expected response of the lattice meshes when statically compressed by a surgeon in a Paprosky 3A situation, see research question 2, is the enduring connection of all struts. The yielding of the meshes will determine the degree to which the designed mesh is able to laterally expand. Diamond based designs with high yielding stresses are expected to provide more lateral expansion in respect to BCC based designs. Moreover, BCC based designs are expected to maintain a non-stochastic structure through a proceeding length/thickness ratio, while diamond based designs will provide an interconnected stochastic structure of buckled struts. The extent of plastic deformation is considerable for each of the BCC- and diamond based designs. However, the diamond based designs will provide plastic deformation at low levels of stress.

4.3 Discussion about the Potential of Osseointegration

To answer sub-question 3.1, the elastic moduli and yield stresses of the different samples were displayed in figure 20. Conclusively, the diamond based designs with a ratio of 10 and 15, and the BCC based designs with a ratio of 15 fitted the defined demands and wishes.

The different lattice based designs showed differences in resulting morphology for impact-, and static uniaxial compression when studying research question 3.2. Given the situation of uniaxial impact, diamond based constructs showed a strong decline in pore size in respect to the BCC based designs. These differences could be explained by the changes in morphology of the samples from a macro-scale perspective. Considering this change in morphology, the BCC based designs showed a less significant change in vertical compression with regard to the diamond based samples. The SLM printing technique is considered an attributing factor in the fast collapse of layers in diamond based designs. Given the higher porosity of diamond meshes, inconsistencies in metallic powder distribution becomes more likely. Additionally, a lower printing angle significantly affects the homogeneity due to overhanging patterns, and thus affecting the mechanical properties of the strut design [46, 47, 48]. These factors weaken the connecting nodes, making them more susceptible to local stresses. At a ratio of 15 the BCC design started to show signals of global buckling. The global buckling is accompanied with a developing compression of pores, see figure 23. This explains the sudden decline in pore size. The more significant decline in pore sizes for diamond based designs is assumed to be a result of the vertical deformation of the samples, see chapter 3.1.1. Vertical deformation is considered a cause of the significant decline in pore size due to the defining of a pore size as the radius of a fitting sphere in a pore. However, cylindrical- and spherical shaped pores can create misconceptions when considering the pore size as a function of a sphere in interpreting the potential of osseointegration. The global buckling and signs of yielding struts in diamond based designs at a ratio of 10, will have contributed to the decline in pore size as well. While the morphology of the BCC based samples could still be identified as rectangular, diamond samples at a ratio of 10 and 15 displayed, while considering the disorganized structure, a more spherical morphology. The stochastic lattice construct and spherical morphology could be most effective in stimulating cellular adhesion. Literature has suggested that porous stochastic structures and spherical shaped pores with varying pore sizes are considered successful in stimulating cell adhesion and in growth of cellular tissue [49, 50]. Therefore the impacted diamond based meshes provides potential in stimulating osseointegration. In the static uniaxial compression test the different lattice types deviated in a resulting morphology as well. The diamond based designs displayed lateral expansion with signs of global-, and local buckling at a ratio of 5. Given a proceeding ratio the diamond samples endured near full vertical compression. The BCC based designs did not show signs of global-, and local buckling, but displayed a collapsion of layer-by-layer throughout the compression process. The Vertical deformations of BCC samples at ratios of 10 and 15 were considered noteworthy, but moderate with respect to the diamond based designs with similar length/thickness ratios. The BCC samples kept the rectangular grid-like pattern resulting in small deviations of morphology in pores. The pore sizes of the BCC samples did decline considerably during static compression, see table 8, in respect to the resulting pore sizes after impact, see table 6.

The potential of the different materials in stimulating osseointegration, see research question 3, was approached from a mechanical- and morphological perspective. The diamond samples with a ratio of 10 and 15, and the BCC samples containing a ratio of 15, possessed yield stresses and elastic moduli most similar to the bone tissue present in a Paprosky 3A situation. During impact the BCC samples maintained the rectangular strut structure and showed modest decline in pore size in respect to the diamond based designs. While the decline in pore size of the diamond based designs are considered to be steep, the disorganized structure of the mesh, and more spherical morphology of the pores could show potential for cellular adhesion. Through static compression the BCC based designs showed a layer-by-layer compression process while the diamond based designs endured near total vertical compression, with the exception of the diamond design containing a ratio of 5.

4.4 Closing Discussion

A proposed design would involve a mesh accustomed to the anatomy of the Paprosky 3A defect. However, as mentioned in chapter 1.1, achieving an ideal fit is challenging. The mesh design will have to be oversized to compensate the densifying of material, and ensure lateral expansion towards the irregular morphology of the defect. A BCC lattice structure with a high length/thickness ratio could provide flexibility in press-fitting the design in the defect. When such a BCC structure is not adequate, post-processing methods like HIP can be applied to enhance ductility. The width and length of the design relative to the defect is challenging to interpret as this research focused on unidirectional lateral expansion and BCC structures are highly anisotropic [51]. An outer hemispherical shaped mesh will be least challenging in covering the width and depth of the fracture before the deformation of the mesh, see figure 33. The top part of the design will consist of a slight hemispherical shell to ensure the imposed stresses are successfully distributed to the outer parts of the mesh and establish seating of the material. The extent of the distributed imposed stresses to the outer parts of the mesh will need to be established through modifications in the yield stresses.

Figure 33: Oversized Mesh

Figure 34: Graded Mesh

The coverage of the bottom surface is most challenging in contrast to the sides of the Paprosky 3A defect and therefore requires more effective lateral expansion. As mentioned in chapters 4.1 and 4.2, a high length/thickness ratio enhances the lateral expansion as long the mesh will not yield and endure plastic deformation. Stresses will be most excessive at the sides of the mesh, due to friction, and top, due to impact- and static forces applied by the surgeon. To ensure sufficing lateral expansion but prevent the yielding of the material, a gradient of the length/thickness ratio can be applied, see figure 34. Research concerning such gradients is currently executed and shows promise in not only lateral expansion, but mimicking the topology and mechanical properties of bone as well [52, 53]. The interaction between the different segments will have to be taken into account. Also, the outer surface of the different segments will differ, affecting the interaction between the mesh and the defect.

After insertion and fixation the cup will need to be inserted. A design challenge is the interaction between the designed mesh and the jumbo cup. A direct interaction could resolve into friction and detachment of metallic particles. Preventing such a safety hazard could be achieved by applying bone cement between the metallic mesh and a ceramic cup, see figure 35. The response of the compressed bone cement and cup will have to be considered in future research.

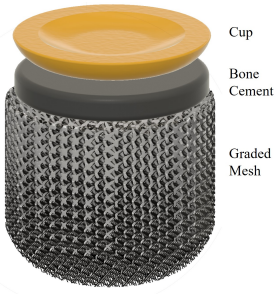

Figure 35: Graded Mesh - Bone Cement - Ceramic Cup

5 Conclusion

To answer the main research question of this study, 3 aspects were taken into account: the material response during uniaxial impact, the material response during uniaxial static compression, and the potential of osseointegration. These aspects were studied by employing uniaxial drop tests, uniaxial compression tests and developing micro-CT scans. Consequently the following conclusions were drawn:

1. During the the uniaxial drop- and static compression test no complete detachment of struts was found.
2. Given an increasing ratio, BCC based designs showed an increase in elastic strain during impact due to the high yield stresses of the material.
3. Given an increasing ratio, diamond based designs showed a decline in elastic strain during impact due to low yield stresses and resulting plastic deformation.
4. The lateral expansion of BCC based designs given a proceeding axial strain are limited by high yield stresses during uniaxial static compression.
5. Diamond based designs at a ratio of 5 show significant lateral expansion through uniaxial static compression, given high yield stresses and unyielding of struts.
6. BCC based designs with a ratio of 15, and diamond based designs containing a ratio of 10 and 15, provided elastic moduli and yield stresses considered comparable with the material properties of bone tissue in a Paprosky 3A defect.
7. BCC based designs show a small decline in pore size with respect to diamond based designs during uniaxial impact.
8. The established decline in pore size was highest in diamond based designs during uniaxial static compression.
9. The diamond based designs with a ratio of 10 and 15 provide potential of osseointegration due to the mesh- and pore morphology.

In response to the main research question and the inclusion of the listed conclusions, BCC based meshes with a high length/thickness ratio and reduced yield stresses are considered most promising in designing an implant to shape and anchor itself in a Paprosky 3A defect without the complete disengagement of struts.

6 Future Research

This study provided an insight in the potential of titanium lattices in revision THA procedures. In proceeding the use of lattice based meshes in the filling of Paprosky 3A defects, future research is required. The capability of predicting resulting peak forces are essential in preventing possible damage to surrounding bone tissue. Variables as elastic moduli, the damping factor and degree of energy absorption are contributing elements and must therefore be considered.

During the uniaxial drop test a growth in elastic strain was established in BCC based designs in respect to an increasing length/thickness ratio. Diamond based designs showed an opposite trend. Establishing a higher elastic strain will enable the orthopaedic surgeon more flexibility in the press-fitting of the material. To what extent enhancing the elastic strain is possible will require analysis concerning the length/thickness ratio of different lattice structures. The preferred resulting flexibility of material will have to be determined in collaboration with orthopaedic surgeons.

Confirming assumptions about probable osseointegration will require the testing, and quantifying, of pore morphology, cellular regeneration and cellular adhesion. Literature considering the quantification of pore morphology remains limited. However, a new approach is issued by Chiang, Martin Y.M. [54]. In this methodology the local thickness methodology and SCL (Star CHord Length) approach are combined and enable the quantification of pore morphology. Conformation of this method will help in establishing a design offering substantial adhesion- and in growth of bone tissue.

The application of a gradient ratio in lattice based designs is a concept with much potential. However, designing such a gradient is challenging due to the many variables present and will require additional research. Difficulties will involve differences in structure, reducing accuracy in SLM printing [55], the simulation of mechanical properties of a graded material through FEM analysis and the testing of long term functionality of a graded implant [56].

Employing bone cement in between the titanium mesh and the cup is assumed to prevent potential safety hazards concerning lose metallic powders. The interaction between these different material structures is not addressed in this study and will therefore require additional attention in future research.

At last the designs will have to be tested with the help of an orthopaedic surgeon. This will require the use of sawbones or most prefereably a cadaver study. Through such studies the response of bone tissue towards the enforced stresses can be observed. FEM models could possibly approach the material characteristics of surrounding bone tissue and make the execution of such experiments less essential. However, bone tissue is anisotropic and the additional loss in density will currently make modeling such simulations most challenging [57]. Moreover, sawbone- or cadaver studies will also create insights in the deformation and load distribution of the designed (graded) meshes.

7 References

[1] Edmund YS Chao et al. "Biomechanical considerations of fracture treatment and bone quality maintenance in elderly patients and patients with osteoporosis". In: *Clinical Orthopaedics and Related Research®* 425 (2004), pp. 12–25.

[2] James W Vaupel. "Biodemography of human ageing". In: *Nature* 464.7288 (2010), pp. 536–542.

[3] Alexander Klug et al. "Future burden of primary and revision hip arthroplasty in Germany: a socio-economic challenge". In: *Archives of Orthopaedic and Trauma Surgery* 141 (2021), pp. 2001–2010.

[4] Steven Kurtz et al. "Projections of primary and revision hip and knee arthroplasty in the United States from 2005 to 2030". In: *Jbjs* 89.4 (2007), pp. 780–785.

[5] Jui-Ting Hsu et al. "The number of screws, bone quality, and friction coefficient affect acetabular cup stability". In: *Medical engineering & physics* 29.10 (2007), pp. 1089–1095.

[6] R. von Eisenhart-Rothe H. Gollwitzer and R. Gradinger. "Aseptic Loosening of Total Hip Replacements - Acetabulum". In: *European Surgical Orthopaedics and Traumatology* (2014), pp. 2553–2572. DOI: https://doi.org/10.1007/978-3-642-34746-7_243.

[7] Wayne G Paprosky, Paul G Perona, and Jeffrey M Lawrence. "Acetabular defect classification and surgical reconstruction in revision arthroplasty: a 6-year follow-up evaluation". In: *The Journal of arthroplasty* 9.1 (1994), pp. 33–44. ISSN: 0883-5403. DOI: https://doi.org/10.1016/0883-5403(94)90135-X.

[8] Mohamed Ghanem et al. "Acetabular defect classification and management: revision arthroplasty of the acetabular cup based on 3-point fixation". In: *Der Orthopade* 49.5 (2020), p. 432. DOI: https://doi.org/10.1007/s00132-020-03895-8.

[9] Jessica JM Telleria and Albert O Gee. "Classifications in brief: Paprosky classification of acetabular bone loss". In: *Clinical Orthopaedics and Related Research®* 471 (2013), pp. 3725–3730.

[10] Han Soul Kim et al. "Revision Total Hip Arthroplasty Utilizing an Acetabular Reinforcement Ring with a Metal Augment: A Minimum Eight-Year Follow-Up Study". In: *Medicina* 59.6 (2023), p. 1036.

[11] L Gaiani et al. "Total hip arthroplasty revision in elderly people with cement and Burch–Schneider anti-protrusio cage". In: *Musculoskeletal Surgery* 93.1 (2009), pp. 15–19.

[12] Nicholas M Brown et al. "The use of structural distal femoral allograft for acetabular reconstruction of Paprosky type IIIA defects at a mean 21 years of follow-up". In: *The Journal of Arthroplasty* 31.3 (2016), pp. 680–683.

[13] GC Babis et al. "High complication rate in reconstruction of Paprosky type IIIa acetabular defects using an oblong implant with modular side plates and a hook". In: *The Journal of Bone & Joint Surgery British Volume* 93.12 (2011), pp. 1592–1596.

[14] K Lingaraj, YH Teo, and N Bergman. "The management of severe acetabular bone defects in revision hip arthroplasty using modular porous metal components". In: *The Journal of Bone & Joint Surgery British Volume* 91.12 (2009), pp. 1555–1560.

[15] Annemiek Groenewoud. "Mechanical properties and deformation behaviour of highly porous pure titanium structures: A first step towards the design of a plastically deformable acetabular implant". In: (2018).

[16] ME Berend et al. "The patient-specific Triflange acetabular implant for revision total hip arthroplasty in patients with severe acetabular defects: planning, implantation, and results". In: *The Bone & Joint Journal* 100.1_Supple_A (2018), pp. 50–54.

[17] GP Goodman and CA Engh Jr. "The custom triflange cup: build it and they will come". In: *The bone & joint journal* 98.1_Supple_A (2016), pp. 68–72.

[18] Christa P de Jonge, Helena MA Kolken, and Amir A Zadpoor. "Non-auxetic mechanical metamaterials". In: *Materials* 12.4 (2019), p. 635.

[19] FSL Bobbert et al. "Additively manufactured metallic porous biomaterials based on minimal surfaces: A unique combination of topological, mechanical, and mass transport properties". In: *Acta biomaterialia* 53 (2017), pp. 572–584.

[20] Shivank A Tyagi and M Manjaiah. "Additive manufacturing of titanium-based lattice structures for medical applications–a review". In: *Bioprinting* 30 (2023), e00267.

[21] Tobias Maconachie et al. "SLM lattice structures: Properties, performance, applications and challenges". In: *Materials & Design* 183 (2019), p. 108137.

[22] Anatoliy Popovich et al. "Producing hip implants of titanium alloys by additive manufacturing". In: *International Journal of Bioprinting* 2.2 (2016).

[23] Gurmohan Singh and Abhineet Saini. "Application of 3D Printing Technology in the Development of Biomedical Implants: A Review." In: *Trends in Biomaterials & Artificial Organs* 35.1 (2021).

[24] Tobias Maconachie et al. "SLM lattice structures: Properties, performance, applications and challenges". In: *Materials & Design* 183 (2019), p. 108137.

[25] Zhuangzhuang Li et al. "3D-Printed Personalized Lattice Implant as an Innovative Strategy to Reconstruct Geographic Defects in Load-Bearing Bones". In: *Orthopaedic Surgery* (2024).

[26] Holden Hyer et al. "High strength WE43 microlattice structures additively manufactured by laser powder bed fusion". In: *Materialia* 16 (2021), p. 101067.

[27] R Pérez, J De Ciurana, and C Riba. "The characterization and specification of functional requirements and geometric tolerances in design". In: *Journal of Engineering Design* 17.4 (2006), pp. 311–324.

[28] Rianne Van Ladesteijn et al. "Mechanical properties of cancellous bone from the acetabulum in relation to acetabular shell fixation and compared with the corresponding femoral head". In: *Medical Engineering & Physics* 53 (2018), pp. 75–81.

[29] Xiaojian Wang et al. "Topological design and additive manufacturing of porous metals for bone scaffolds and orthopaedic implants: A review". In: *Biomaterials* 83 (2016), pp. 127–141.

[30] HMA Kolken et al. "Additively manufactured space-filling meta-implants". In: *Acta Biomaterialia* 125 (2021), pp. 345–357.

[31] Granta Design. *Granta EduPack*. Version 23.2.1. Granta Design, 2023. URL: https://www.grantadesign.com/products/edupack/.

[32] Ruben Doyle et al. "An in vitro model of impaction during hip arthroplasty". In: *Journal of Biomechanics* 82 (2019), pp. 220–227.

[33] Andreas Fritsche et al. "Experimental investigations of the insertion and deformation behavior of press-fit and threaded acetabular cups for total hip replacement". In: *Journal of Orthopaedic Science* 13 (2008), pp. 240–247.

[34] Shivank A Tyagi and M Manjaiah. "Additive manufacturing of titanium-based lattice structures for medical applications–a review". In: *Bioprinting* 30 (2023), e00267.

[35] SM Ahmadi et al. "Mechanical behavior of regular open-cell porous biomaterials made of diamond lattice unit cells". In: *Journal of the mechanical behavior of biomedical materials* 34 (2014), pp. 106–115.

[36] J Magré et al. "Deformable titanium for acetabular revision surgery: a proof of concept". In: *3D Printing in Medicine* 9.1 (2023), p. 16.

[37] *Mimics*. Version 26.0. Materialise Magics. URL: https://www.materialise.com/en/industrial/software/magics-data-build-preparation?gad_source=1&gclid=Cj0KCQjwir2xBhC_ARIsAMTXk847_JwZn3bUcMmuprL9etouP5MOziNi7ZL9Ol4ICwtdql-KW8PQlAkaAvGpEALw_wcB.

[38] International Organization for Standardization. *ISO 2439:2008 Flexible cellular polymeric materials — Determination of hardness (indentation technique), number = ISO 2439:2008, institution = ISO, year = 2008,* tech. rep.

[39] International Organization for Standardization. *ISO 13314:2012 Mechanical testing of metals - Ductility testing - Compression test for porous and cellular metals, number = ISO 13314:2012, institution = ISO, year = 2012,* tech. rep.

[40] *3-MAtic*. Version 18.0. Materialise Magics. URL: https://www.materialise.com/en/industrial/software/magics-data-build-preparation?gad_source=1&gclid=Cj0KCQjwir2xBhC_ARIsAMTXk847_JwZn3bUcMmuprL9etouP5MOziNi7ZL9Ol4ICwtdql-KW8PQlAkaAvGpEALw_wcB.

[41] Thomas Tancogne-Dejean and Dirk Mohr. "Stiffness and specific energy absorption of additively-manufactured metallic BCC metamaterials composed of tapered beams". In: *International Journal of Mechanical Sciences* 141 (2018), pp. 101–116.

[42] Zuhal Ozdemir et al. "Energy absorption in lattice structures in dynamics: Experiments". In: *International Journal of Impact Engineering* 89 (2016), pp. 49–61.

[43] Xingchen Yan et al. "Effect of hot isostatic pressing (HIP) treatment on the compressive properties of Ti6Al4V lattice structure fabricated by selective laser melting". In: *Materials Letters* 255 (2019), p. 126537.

[44] Xingchen Yan et al. "Microstructural and mechanical optimization of selective laser melted Ti6Al4V lattices: Effect of hot isostatic pressing". In: *Journal of Manufacturing Processes* 77 (2022), pp. 151–162.

[45] Joëll Magré. "Deformable Acetabular Cups: A biomechanical proof of concept". Thesis. 2020.

[46] Bartłomiej Wysocki et al. "Microstructure and mechanical properties investigation of CP titanium processed by selective laser melting (SLM)". In: *Journal of Materials Processing Technology* 241 (2017), pp. 13–23.

[47] S Murchio et al. "Additively manufactured Ti–6Al–4V thin struts via laser powder bed fusion: Effect of building orientation on geometrical accuracy and mechanical properties". In: *Journal of the Mechanical Behavior of Biomedical Materials* 119 (2021), p. 104495.

[48] MR Costa, A Sohouli, and A Suleman. "Multi-scale and multi-material topology optimization of gradient lattice structures using surrogate models". In: *Composite Structures* 289 (2022), p. 115402.

[49] Zhuangzhuang Li et al. "3D-Printed Personalized Lattice Implant as an Innovative Strategy to Reconstruct Geographic Defects in Load-Bearing Bones". In: *Orthopaedic Surgery* 16.4 (2024), pp. 821–829.

[50] Zhuangzhuang Li et al. "Biomimetic design and clinical application of Ti-6Al-4V lattice hemipelvis prosthesis for pelvic reconstruction". In: *Journal of Orthopaedic Surgery and Research* 19.1 (2024), p. 210.

[51] Miao Zhao et al. "Design, mechanical properties, and optimization of BCC lattice structures with taper struts". In: *Composite Structures* 295 (2022), p. 115830.

[52] William Van Grunsven et al. "Fabrication and mechanical characterisation of titanium lattices with graded porosity". In: *Metals* 4.3 (2014), pp. 401–409.

[53] Naresh Koju, Suyash Niraula, and Behzad Fotovvati. "Additively manufactured porous Ti6Al4V for bone implants: a review". In: *Metals* 12.4 (2022), p. 687.

[54] Martin YM Chiang et al. "Local thickness and anisotropy approaches to characterize pore size distribution of three-dimensional porous networks". In: *Tissue Engineering Part C: Methods* 15.1 (2009), pp. 65–76.

[55] Lei Yang et al. “An investigation into the effect of gradients on the manufacturing fidelity of triply periodic minimal surface structures with graded density fabricated by selective laser melting”. In: *Journal of Materials Processing Technology* 275 (2020), p. 116367.

[56] Dalia Mahmoud and Mohamed A Elbestawi. “Lattice structures and functionally graded materials applications in additive manufacturing of orthopedic implants: a review”. In: *Journal of Manufacturing and materials Processing* 1.2 (2017), p. 13.

[57] Joyce H Keyak et al. “Prediction of femoral fracture load using automated finite element modeling”. In: *Journal of biomechanics* 31.2 (1997), pp. 125–133.